^{1}H NMR Investigation of Paramagnetic Chromium(III) Olefin Polymerization Catalysts: Experimental Results, Shift Assignment and Prediction by Quantum Chemical Calculations†

Pablo Fernández,‡ Hans Pritzkow,‡ Jorge J. Carbó,§,|| Peter Hofmann,§ and Markus Enders*,‡

Anorganisch- and Organisch-Chemisches Institut der Ruprecht-Karls-Universität Heidelberg, Im Neuenheimer Feld 270, D-69120 Heidelberg, Germany, and Departament de Química Física i Inorgànica, Universitat Rovira i Virgili, Marcel lí Domingo s/n, 43007 Tarragona, Spain

Received February 23, 2007

The new paramagnetic quinolyl-functionalized Cp chromium(III) complexes **4**−**8**, which serve as precursors for highly active olefin polymerization catalysts, have been synthesized and were investigated together with the known complexes **1**−**3** by ^{1}H NMR. Full assignment of the observed NMR signals in these systems was achieved by comparison of the different spectra and by spin unrestricted density functional calculations (UB3LYP level) of the Fermi contact term at the hydrogen atoms. All the geometries were optimized using the experimentally determined solid-state molecular structures as starting points. We obtained a very good correlation ($r^2 = 0.97$) between calculated Fermi contact spin densities at the UB3LYP/6-311G(d) level and experimental paramagnetic ^{1}H NMR shifts. Polarization basis set functions at heavy elements are required to reproduce experimental results, whereas polarization functions at hydrogen atoms and/or diffuse functions do not improve the results. The good correlation between calculated and experimental results indicates that the experimental hyperfine shifts are dominated by Fermi contact interactions. Nevertheless, we were able to identify and estimate non-negligible dipolar contributions to the chemical shifts for some protons. It is possible to predict ^{1}H NMR shifts of similar organometallic compounds and to obtain structural information of in situ generated paramagnetic species, which play a key role in several catalytic transformations with paramagnetic catalysts. Additionally, calculations provided us with detailed information of the spin density distribution along the molecular systems.

Introduction

Besides the well-established heterogeneous Ziegler−Natta catalysts,[1] chromium-based heterogeneous systems are among the most important industrial catalysts for the polymerization of α-olefins.[2] Whereas homogeneous group 4 catalysts are also well-established and already in industrial use, homogeneous chromium analogues have been investigated much less. However, some chromium(III) complexes show excellent polymerization activities and allow for the synthesis of useful homo- and copolymers of ethylene and α-olefins.[3,4] For further control of catalyst properties, it is necessary to have a powerful tool for the spectroscopic investigation of catalyst/cocatalyst combinations in the presence of reactive substrates. With diamagnetic catalyst/cocatalyst systems, this has been achieved by NMR studies that have led to a detailed knowledge of initiation, propagation, and termination steps of the polymerization process.[5] In the case of chromium(III)-based compounds, the paramagnetic character leads to strong shifts and broadening of the NMR signals.[6] In addition, the assignment of experimental

† Dedicated to Prof. Roald Hoffmann on the occasion of his 70th birthday.

* To whom correspondence should be addressed. Tel.: +49-6221-546247; fax: +49-6221-541616247; e-mail: markus.enders@uni-hd.de.

‡ Anorganisch-Chemisches Institut, Ruprecht-Karls-Universität Heidelberg.

§ Organisch-Chemisches Institut, Ruprecht-Karls-Universität Heidelberg.

|| Universitat Rovira i Virgili.

(1) (a) Ziegler, K.; Holzkamp, E.; Breil, H.; Martin, H. *Angew. Chem., Int. Ed.* **1955**, *67*, 426. (b) Natta, G.; Pino, P.; Corradini, P.; Danusso, F.; Mantica, E.; Mozzanti, G.; Moraglio, G. *J. Am. Chem. Soc.* **1955**, *77*, 1708. (c) Wilke, G. *Angew. Chem., Int. Ed.* **2003**, *42*, 4996.

(2) (a) Hogan, J. P.; Banks, R. L. Polymers and Production thereof. Belgian Patent 530,617,1955 and U.S. Patent 2825,721, Phillips Petroleum Co., 1958. (b) Hogan, J. P. *J. Polym. Sci., Part A: Polym. Chem.* **1970**, *8*, 2637. (c) Karapinka, G. L. Polymerization of Ethylene using supported Bis-(cyclopentadienyl) Chromium(II) Catalysts. U.S. Patent 3,709,853, 1973. (d) Karol, F. L.; Karapinka, G. L.; Wu, C.; Dow, A. W.; Johnson, R. N.; Garrick, W. L. *J. Polym. Sci., Part A: Polym. Chem.* **1972**, *10*, 2621.

(3) (a) Theopold, K. H. *Acc. Chem. Res.* **1990**, *23*, 263. (b) Theopold, K. H. *Eur. J. Inorg. Chem.* **1998**, *1*, 15. (c) Köhn, R. D.; Haufe, M.; Mihan, S.; Lilge, D. *Chem. Commun.* **2000**, 1927. (d) Döhring, A.; Göhre, J.; Jolly, P. W.; Kryger, B.; Rust, J.; Verhovnik, G. P. J. *Organometallics* **2000**, *19*, 388. (e) McGuinness, D. S.; Gibson, V. C.; Wass, D. F.; Steed, J. W. *J. Am. Chem. Soc.* **2003**, *125*, 12716. (f) Esteruelas, M. A.; López, A. M.; Méndez, L.; Oliván, M.; Oñate, E. *Organometallics* **2003**, *22*, 395. (g) Zhang, H.; Ma, J.; Qian, Y.; Huang, J. *Organometallics* **2004**, *23*, 5681. (h) Small, B. L.; Carney, M. J.; Holman, D. M.; O'Rourke, C. E.; Halfen, J. A. *Macromolecules* **2004**, *37*, 4375. (i) Esteruelas, M. A.; López, A. M.; Méndez, L.; Oliván, M.; Oñate, E. *Organometallics* **2003**, *22*, 395. (j) McGuinness, D. S.; Gibson, V. C.; Wass, D. F.; Steed, J. W. *J. Am. Chem. Soc.* **2003**, *125*, 2716. (k) Jones, D. J.; Gibson, V. C.; Green, S. M.; Maddox, P. J.; White, A. J. P.; Williams, D. J. *J. Am. Chem. Soc.* **2005**, *127*, 11037.

(4) (a) Enders, M.; Mihan, S.; Lilge, D.; Schweier, G. Co-Polymers of Ethylene with C3-C9 α-Olefins. PCT Int. Appl., WO 0112687 A1, 1999. (b) Enders, M.; Fernández, P.; Ludwig, G.; Pritzkow, H. *Organometallics* **2001**, *20*, 5005. (c) Mihan, S.; Lilge, D.; De Lange, P.; Schweier, G.; Schneider, M.; Rief, U.; Handrich, U.; Hack, J.; Enders, M.; Ludwig, G.; Rudolph, R. Monocyclopentadienyl Complexes of Chromium, Molybdenum and Tungsten with a Donor Bridge. U.S. Patent 6,437,161 B1, 2001. (d) Kohl, G.; Enders, M.; Pritzkow, H. *Organometallics* **2004**, *23*, 3832.

(5) (a) Li, L.; Stern, C. L.; Marks, T. J. *Organometallics* **2000**, *19*, 3332. (b) Bryliakov, K. P.; Semikolenova, N. V.; Zakharov, V. A.; Talsi, E. P. *J. Organomet. Chem.* **2003**, *683*, 23. (c) Bryliakov, K. P.; Talsi, E. P.; Bochmann, M. *Organometallics* **2004**, *23*, 149. (d) Deck, P. A.; Konaté, M. M.; Kelly, B. V.; Slebodnick, C. *Organometallics* **2004**, *23*, 1089. (e) Shapiro, P. J.; Cotter, W. D.; Schaefer, W. P.; Labinger, J. A.; Bercaw, J. E. *J. Am. Chem. Soc.* **1994**, *116*, 4623. (f) Shultz, L. H.; Tempel, D. J.; Brookhart, M. *J. Am. Chem. Soc.* **2001**, *124*, 11539.

10.1021/om070173y CCC: $37.00
Publication on Web 07/25/2007

NMR shifts even for known compounds is not always possible. This leads to the belief that NMR spectroscopy is less useful for the characterization of paramagnetic compounds. Therefore, literature often does not report NMR shift data of such molecules, although it is often quite easy to obtain their ^{1}H NMR spectra.[7]

The study of homogeneous diamagnetic Ziegler−Natta catalysts by NMR is widespread and provides valuable information about the properties of the active species. In many cases, the catalysts have to be activated with a cocatalyst, so that significant overlap of the NMR signals of the catalyst and the cocatalyst has to be avoided. Therefore, these investigations are generally carried out with nonstandard activating agents and/or isotopically marked systems. If methylaluminoxane (MAO) is used for the activation, at least 50 equiv of Al per catalyst molecule is necessary. Thus, the normal window for ^{1}H NMR is dominated by the excess of cocatalyst. In these cases, paramagnetic systems could be advantageous for NMR studies, as the NMR signals are often much more shifted, and therefore, overlap with the signals of diamagnetic species is less important. In paramagnetic molecules, unpaired electrons generally lead to significant electron spin polarizations at nuclei well apart from the center of paramagnetism (which is usually at the metal atom). The residual unpaired electron density at these positions shield or deshield the nuclear spins. Consequently, the NMR signals of the nuclei are shifted to higher or lower frequencies, depending on whether the spin density is positive or negative. This allows for the observation of signals far apart from the normal diamagnetic region, which could provide valuable information about the metal environment of trialkylaluminium- and MAO-activated catalysts. In fact, for some paramagnetic chromium complexes, systematic NMR investigations were carried out, mainly by Köhler et al.[7b] From these studies on mono- and bimetallic complexes, the authors obtained spin density maps of several molecules, assignments, and interpretations of ^{1}H and ^{13}C NMR data. However, it is difficult and sometimes even impossible to predict paramagnetic shifts of organometallic compounds.

In many cases, the Fermi contact interactions dominate the paramagnetic shifts experienced by NMR active nuclei. Thus, numerous calculations of Fermi contact coupling constants based on ab initio and density functional methods have been reported to predict the hyperfine shifts.[8] The theoretical studies have mainly focused on small organic paramagnetic systems,[9] whereas the application to transition metal-based systems has been accomplished only recently by a few groups.[10]

During the last few years, we have reported the synthesis and characterization of a set of amino-functionalized Cp-based chromium(III) complexes.[4] Treatment of these compounds with MAO gives highly active catalysts for olefin polymerization, which are very stable at high temperatures. To date, these complexes have been analyzed by techniques other than NMR, mostly due to the difficulty of signal assignments in these paramagnetic systems. Whereas compounds studied by Köhler et al. have up to five different ^{1}H NMR signals, complexes **1**−**4** have already eight and **5**−**8** up to 11 ^{1}H NMR signals (Chart 1). However, due to the rigidity of these complexes, molecular structures obtained by DFT calculations should be able to match well the species present in solution.

Herein, we report the synthesis and characterization of several new quinolyl−Cp-based chromium(III) complexes (**4**−**8**). The characterization includes X-ray diffraction and paramagnetic ^{1}H NMR analysis. In addition, we have carried out DFT calculations on **1**−**8** to obtain the unpaired electron spin density distributions that can be correlated with experimental NMR data.

Chart 1. Chromium(III) Complexes Studied in This Paper

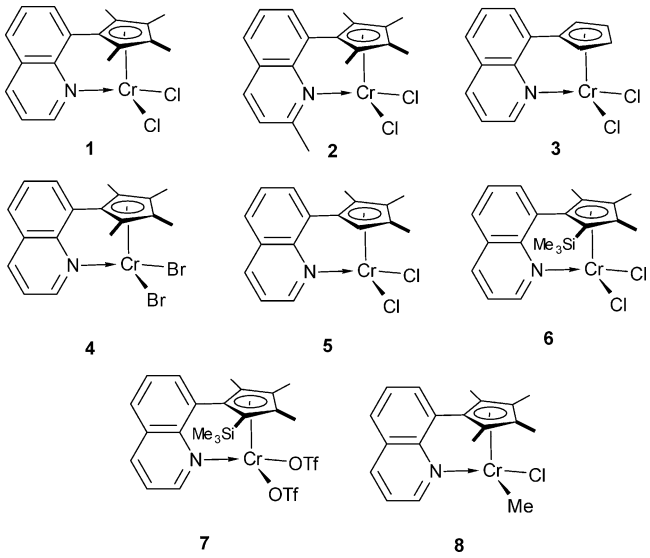

Chart 2. Quinolyl−Cyclopentadienyl Ligands Reported Prior to This Paper

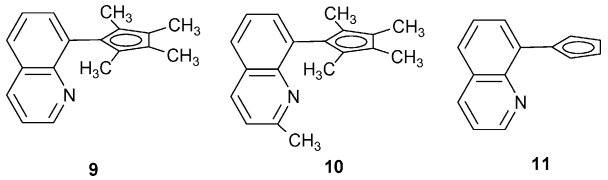

Results and Discussion

Ligand Synthesis. The preparation and characterization of the quinolyl−cyclopentadienes **9H**−**11H** (Chart 2) follow different routes, which have already been reported by us.[11] The new ligand precursor **12H** was obtained by a one-step route from 8-lithioquinoline and 2,3,4-trimethylcyclopent-2-enone

(6) (a) La Mar, G. N.; Horrocks, W., Jr.; Holms, R. H. *NMR of Paramagnetic Molecules: Principles and Applications*; Academic Press: New York, 1973. (b) Bertini, I.; Luchinat, C.; Parigi, G. *Solution NMR of Paramagnetic Molecules*; Elsevier: Amsterdam, 2001. (c) Köhler, F. H. *Magnetism: Molecules to Materials*; Wiley-VCH Verlag GmbH: Weinheim, Germany, 2001; p 379. (d) Wilkens, S. J.; Xia, B.; Weinhold, F.; Markley, J. L.; Westler, W. M. *J. Am. Chem. Soc.* **1998**, *120*, 4806.

(7) (a) Heintz, R. A.; Neiss, T. G.; Theopold, K. H. *Angew. Chem., Int. Ed.* **1994**, *106*, *22*, 2389. (b) Bräunlein, B.; Köhler, F. H.; Strauss, W.; Zeh, H. *Z. Naturforsch., B: Chem. Sci.* **1995**, *50*, 1739.

(8) Kaupp, M.; Bühl, M.; Malkin, V. G. *Calculation of NMR and EPR Parameters: Theory and Applications*; Wiley-VCH: Weinheim, Germany, 2004.

(9) (a) Barone, V.; Adamo, C.; Russo, N. *Chem. Phys. Lett.* **1993**, *212*, 5. (b) Eriksson, L. A.; Malkina, O. L.; Malkin, V. G.; Salahub, D. R. *J. Chem. Phys.* **1994**, *100*, 5066. (c) Cohen, M. J.; Chong, D. P. *Chem. Phys. Lett.* **1995**, *234*, 405. (d) Adamo, C.; Barone, V.; Fortunelli, A. *J. Chem. Phys.* **1995**, *102*, 384. (e) O'Malley, P. J.; Collins, S. J. *Chem. Phys. Lett.* **1996**, *259*, 296.

(10) (a) Wilkens, S. J.; Xia, B.; Weinhold, F.; Markley, J. L.; Westler, W. M. *J. Am. Chem. Soc.* **1998**, *120*, 4806. (b) Mao, J.; Zhang, Y.; Oldfield, E. *J. Am. Chem. Soc.* **2002**, *124*, 13911. (c) Sporer, C.; Heise, H.; Wurst, K.; Ruiz-Molina, D.; Kopacka, H.; Jaitner, P.; Köhler, F. H.; Novoa, J. J.; Veciana, J. *Chem.—Eur. J.* **2004**, *10*, 1355. (d) Zhang, Y.; Sun, H.; Oldfield, E. *J. Am. Chem. Soc.* **2005**, *127*, 3652. (e) Machonkin, T. E.; Westler, W. M.; Markley, J. L. *Inorg. Chem.* **2005**, *44*, 779. (f) Paul, F.; da Costa, G.; Bondon, A.; Gauthier, N.; Sinbandhit, S.; Toupet, L.; Costuas, K.; Halet, J. F.; Lapinte, C. *Organometallics* **2007**, *26*, 874.

(11) (a) Enders, M.; Rudolph, R.; Pritzkow, H. *Chem. Ber.* **1996**, *129*, 459. (b) Enders, M.; Kohl, G.; Pritzkow, H. *Organometallics* **2002**, *21*, 1111. (c) Mihan, S.; Enders, M.; Kohl, G. Method for Producing Cyclopentadienyl Complexes. PCT Int. Appl., WO2002074745 A1, 2002.

Scheme 1. Synthesis of 12H and 13H

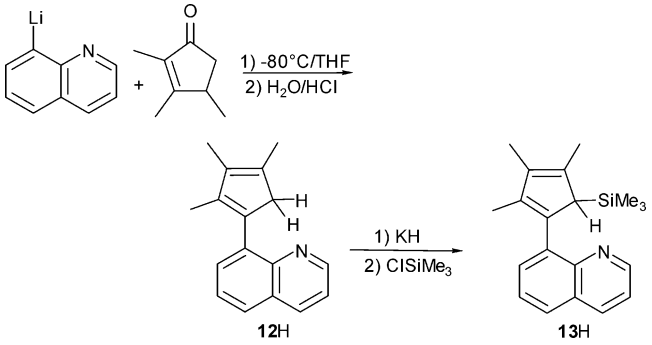

Scheme 2. Synthesis of 1−7

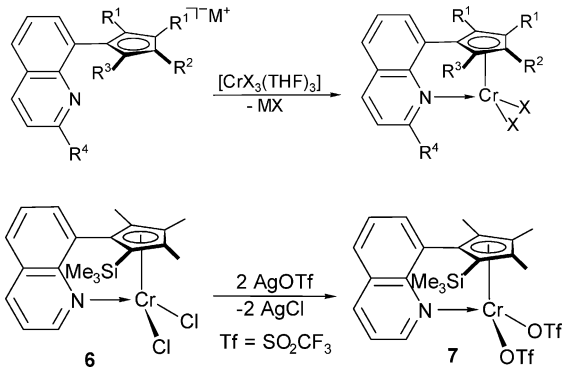

Table 1. Substitution Pattern of Compounds Investigated

complex	ligand	X	R^1	R^2	R^3	R^4
1	**9**	Cl	CH_3	CH_3	CH_3	H
2	**10**	Cl	CH_3	CH_3	CH_3	CH_3
3	**11**	Cl	H	H	H	H
4	**9**	Br	CH_3	CH_3	CH_3	H
5	**12**	Cl	CH_3	CH_3	H	H
6	**13**	Cl	CH_3	CH_3	$Si(CH_3)_3$	H
7	**13**	OTf	CH_3	CH_3	$Si(CH_3)_3$	H
8	**9**	Cl/CH_3	CH_3	CH_3	CH_3	H

(Scheme 1). This cyclopentadiene derivative is a valuable precursor for the introduction of different groups at the Cp ring through a deprotonation/electrophile addition sequence. This is exemplified by the synthesis of the trimethylsilyl derivate **13H**. 1,2,3-Trimethyl-4(8-quinolyl)cyclopentadiene (**12H**) was deprotonated with potassium hydride to give the corresponding potassium salt. Addition of chlorotrimethylsilane leads to **13H**, which was purified by distillation.

Synthesis and Characterization of the Chromium Complexes 4−8. We have already reported the synthesis and characterization of the chromium(III) complexes **1**−**3**.[4] The dibromo derivate **4** as well as the new complexes **5** and **6** can be obtained easily from the reaction of the respective potassium cyclopentadienides with $[CrBr_3(THF)_3]$ or $[CrCl_3(THF)_3]$ (Scheme 2 and Table 1). From the ligands **12** and **13**, **5** and **6** were synthesized in a similar way. The triflate derivate **7** was obtained by exchange of the chloro ligands in **6** with silver trifluoromethylsulfonate (Scheme 2).

The new complexes **4**−**7** were all characterized by single-crystal X-ray crystallography and by mass spectrometry. The geometries of the **4**−**7** are quite similar. The rigid chelating ligands define the coordination sphere of the metal atoms. As an example, a picture of **7** is shown in Figure 1. The almost planar quinolyl moiety and the plane defined by the carbon atoms of the Cp ring are practically orthogonal. The typical three-legged piano-stool arrangement for $CpML_3$ complexes is not found in **4**−**7** as the nitrogen atom is shifted toward the Cp

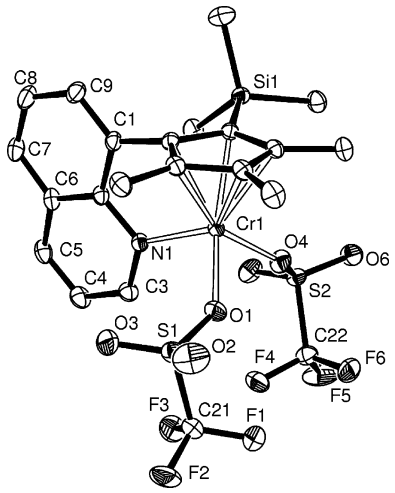

Figure 1. Solid-state molecular structure of **7**. Geometries of **4**−**6** are very similar (see Supporting Information for details).

Scheme 3. Reaction of 9K with $[CrCl_2Me(THF)_3]$

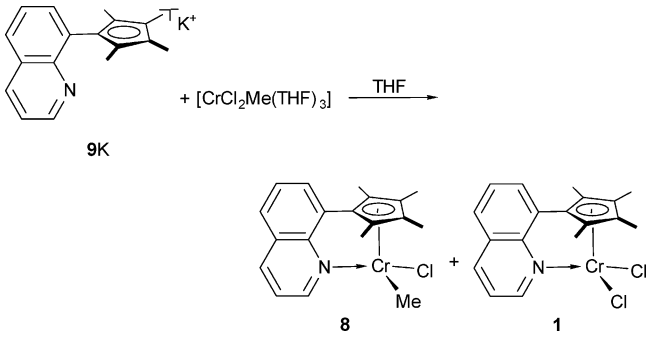

plane. This geometry shift may be expressed by the difference in the distances from the plane of the Cp ring to the chromium atom and to the nitrogen atom. As a reference, this value is 1.03 Å in the complex $Cp^*CrCl_2(C_3H_4N_2)$,[12] whereas in **4**−**7**, values of 0.69−0.73 Å are observed.

Recently, we have reported unexpected alkylation reactions for **1** and **2**.[13] Whereas organolithium as well as Grignard reagents lead to alkylation at the ligand, MAO only reacts at the metal center. As the formation of the metal−alkyl or −hydride is required for the activation of the catalysts, we were interested in the synthesis of chloro−alkyl derivates of our complexes. Abstraction of a chloride anion from these compounds should lead to active catalysts without the addition of an alkylating agent. We therefore treated $[CrCl_2Me(THF)_3]$[14,15] with the potassium salt **9K** (Scheme 3). The mass spectrum shows that a mixture of the desired compound **8** together with the dichloro derivate **1** is present. To purify the compound, crystals were grown in a two-phase system of dichloromethane layered with toluene. However, the MS analysis shows again the existence of a mixture of **8** and **1**. The single-crystal X-ray analysis proves that one of the chlorine atoms of **1** is partially substituted by a methyl group in the crystal with a ratio of $Cl/CH_3 = 0.61:0.39$. Only one of the two chlorine positions in **1**

(12) (a) Rojas, R.; Valderrama, M.; Garland, M. T. *J. Organomet. Chem.* **2004**, *689*, 293. (b) Cambridge Structural Database, reference code ARIROI. (c) Allen, F. H.; Kennard, O. *Chem. Des. Automat. News* **1993**, *8*, 31.

(13) Enders, M.; Fernández, P.; Mihan, S.; Pritzkow, H. *J. Organomet. Chem.* **2003**, *687*, 125.

(14) Nishimura, K.; Kuribayashi, H.; Yamamoto, A.; Ikeda, S. *J. Organomet. Chem.* **1972**, *37*, 499.

(15) Single-crystal X-ray determination of $CrCl_2CH_3(THF)_3$ was performed. The THF ligands were arranged in a meridional manner. Details of the structure determination are reported in the Supporting Information.

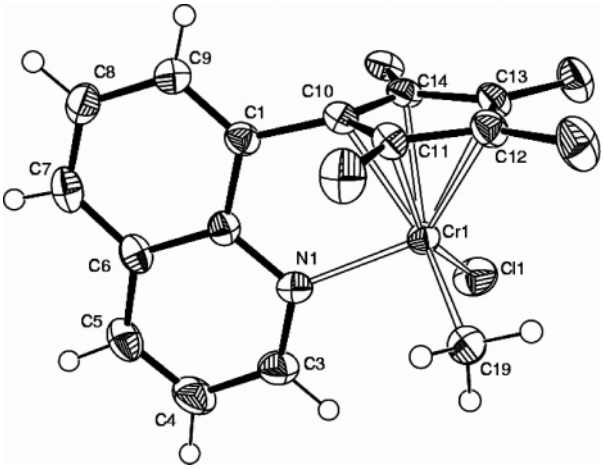

Figure 2. Solid-state molecular structure of **8**. Hydrogens at the Cp methyl groups are not shown for clarity.

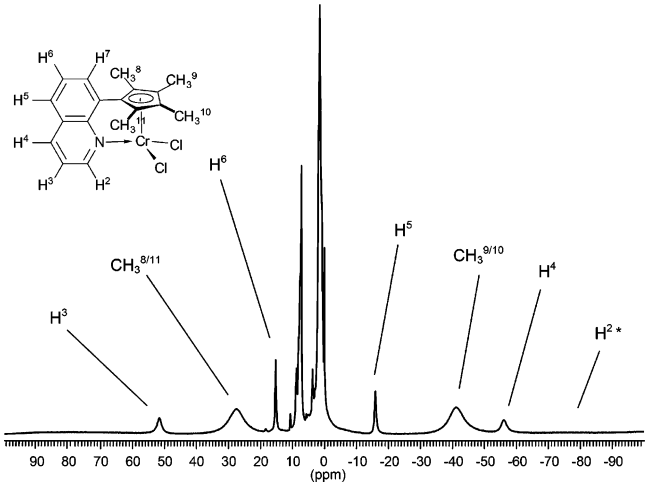

Figure 3. ^{1}H NMR spectrum of **1** in $CDCl_3$ (295 K, 200 MHz). Asterisks show signal for H^2 only visible after amplification.

is statistically occupied by CH_3 groups (see Figure 2). The substitution of a chlorine atom in **1** by a CH_3 group (**8**) therefore does not lead to significant changes in the geometry of the complex. All intramolecular atom distances and angles in the cocrystal **1**/**8** are practically identical with the values from the previous single-crystal structure determination of **1**.[4b]

Paramagnetic ^{1}H NMR of the Chromium Complexes 1−8. The ^{1}H NMR of **1** in $CDCl_3$ at room temperature (Figure 3) shows six resonances outside the diamagnetic region (0−10 ppm), although a total of eight signals is expected. Resonances in the 0−10 ppm region are difficult to assign because they may be hidden by residual solvent signals or diamagnetic impurities. Integration allows the assignment of the signals at 27.6 and −41.1 ppm to the methyl groups at the Cp ring (six H atoms as compared to one H atom for the other signals). At first sight, the chemical shifts of the methyl groups with negative and positive signs are unexpected, as the number of bonds between the H atoms and the Cr^{3+} center are identical, and therefore, the signs of the spin densities should also be the same. However, a similar behavior was reported for octamethyldiphosphachromocene, where the phosphorus atoms lead to a lower symmetry.[16] In **1**, the coordination of the quinoline moiety to the chromium center leads to the fixation of the Cp ring orientation relative to the orbitals of the $CrCl_2$ fragment. This

(16) Feher, R.; Köhler, F. H.; Nief, F.; Ricard, L.; Rossmayer, S. *Organometallics* **1997**, *16*, 4606.

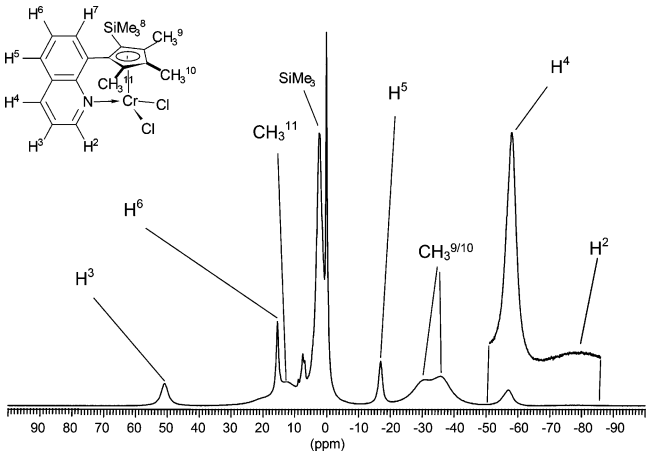

Figure 4. ^{1}H NMR spectrum of **6** in $CDCl_3$ (295 K, 200 MHz).

allows for the alternation of spin density in the η^5 bonded ring. To the best of our knowledge, the quinolyl−cyclopentadienyl systems are the first paramagnetic Cp complexes where positive and negative ^{1}H NMR shifts for the CH_3 substituents are reported. In the case of **3**, the signals of the hydrogen atoms directly attached to the cyclopentadienyl ring lie in the region of 240−340 ppm.[4d] These values are comparable with the shift found for the corresponding Cp−H signal in $CpCrCl_2(C_5H_5N)$.[7b]

The other four signals observed in the spectrum of **1** have a lower intensity and belong to four protons of the quinoline (Figure 3). By amplification, a very broad resonance is visible at about −80 ppm, which results from the H^2 proton that has the shortest distance to the paramagnetic chromium center (3.071 Å). The signals in the heterocyclic part of the quinoline can be compared with the results obtained for dichlorocyclopentadienyl−pyridinechromium(III) by Köhler,[7b] who assigned the peaks at −36.4, 11.0, and −39.4 ppm to the protons at positions ortho, meta, and para on the pyridine, respectively. As reported, this is consistent with a typical feature of the Fermi contact shift: the sign changes with the number of bonds between the paramagnetic center and the observed nucleus.[6] For an odd number of bonds, a negative spin density and therefore a negative contact shift is expected, whereas for an even number of bonds, the inverse signs should be observed. In our case, the hydrogen atom at position 2 of the quinoline is close to the metal so that both dipole−dipole interactions and Fermi contact shift may contribute to the chemical shift and line broadening. The line broadening associated with the dipolar shift is proportional to r^{-6}, r being the distance between the paramagnetic center and the nucleus under study.[6] This fact supports the assumption that the very broad signal at −78 ppm corresponds to the hydrogen atom of the quinoline closest to the metal (H^2) and that the signals at 50.6 and −55.6 ppm can be assigned to protons at positions 3 and 4 of the quinoline, respectively. The last two signals at 15.3 and −16.4 ppm are from two protons of the homocyclic part of the quinoline. The third signal is not observed and possibly hidden in the diamagnetic region.

In the case of the trimethylsilyl derivate **6**, the ^{1}H NMR (Figure 4) shows similar features, but the methyl groups at positions 9 and 10 of the Cp are separated into two signals at −27.3 and −36.7 ppm, respectively. The protons of the trimethylsilyl group are further apart from the paramagnetic center and therefore located in the diamagnetic region. The third methyl group of the Cp is not clearly visible, but its position can be determined by acquiring spectra at different temperatures (see Supporting Information). Higher temperatures lead to signal

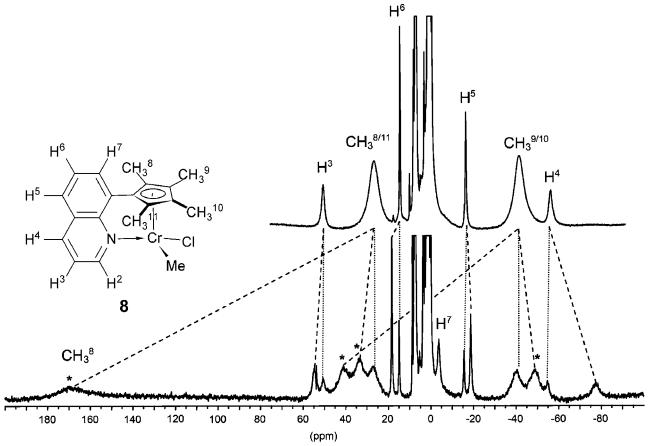

Figure 5. ^{1}H NMR spectra in $CDCl_3$ (295 K, 200 MHz) of **1** (top) and reaction product of **9K** with [$CrCl_2Me(THF)_3$] (bottom). The dotted lines connect signals of **1**, while the dashed lines point to corresponding signals in **8**. Asterisks show the signals of the four nonequivalent CH_3 groups in **8** (for assignments, see text).

sharpening and a shift toward the diamagnetic region. This improves the separation of the methyl signals, and the broad resonance in the range of 10−15 ppm can be assigned to the methyl protons at position 11 of the Cp. This temperature dependence is due to a change in the population of the electron spin orientations parallel and antiparallel to the external magnetic field and leads to magnetic behavior as described by the Curie Law. The temperature dependence in the ^{1}H NMR spectra of **6** indeed obeys the Curie Law (i.e., T^{-1} dependence), which shows that this complex is a monomer in solution. If dimers were present, a magnetic coupling of the paramagnetic center should lead to deviations, as observed for $[(C_5H_5)CrCl_2]_2$.[7b]

The ^{1}H NMR of triflate derivate **7** is similar to that of the dichloro precursor **6**, but the paramagnetic shifts are smaller. Whereas the assignments of the ^{1}H NMR signals in **1**−**7** are consistent and in accordance with values reported for similar compounds, the ^{1}H NMR signal of **8** is more difficult to interpret. As shown by MS analysis and X-ray diffraction, **8** is contaminated by **1**. The signals for **1** can be easily identified in the mixture of **1** and **8**. Integration allows the estimation of the ratio between complexes **8** and **1** to be 2:1 in the sample. The signals of the quinoline protons of **8** can be identified easily (see dashed lines in Figure 5). The paramagnetic shifts in **8** are larger as compared to the shifts in **1**. The Fermi contact shift is notably stronger at H^4, which is in a para position relative to the metal. A new signal appears at −4 ppm, which belongs to H^7. In **1**, this resonance was hidden in the diamagnetic region. The signal of the chromium bonded CH_3 group is not visible as it is very close to the paramagnetic center and therefore strongly shifted and extremely broadened. The assignment of the Cp−methyl groups is more difficult. On going from **1** to **8**, the mirror plane disappears, and consequently, the former two signals split into four. Three of the latter signals lie in the expected −50 to +50 ppm range, whereas the fourth signal appears at a very low field (asterisks in Figure 5). Although we are able to identify the four methyl groups of **8**, we cannot easily assign them. The total assignment of ^{1}H NMR signals for this and other difficult cases is achieved with the help of quantum mechanics calculations.

Theoretical Prediction of Paramagnetic ^{1}H NMR Chemical Shifts. The chemical shift in paramagnetic compounds can be divided into two terms

$$\delta_{obs} = \delta_{dia} + \delta_{para} \quad (1)$$

where δ_{obs}, δ_{dia}, and δ_{para} are the observed, diamagnetic, and paramagnetic shifts, respectively. δ_{dia} is the shift that would be observed in the absence of unpaired electrons and is in our case taken to be the shift value of analogous diamagnetic complexes (i.e., $\delta_{dia} = 2$ ppm for a CH_3 group at the Cp ring and $\delta_{dia} = 8$ ppm for the protons at the quinoline).[10a] On the other hand, the paramagnetic shift, δ_{para}, is the sum of the Fermi contact (δ_{con}) and the dipolar contribution (δ_{dip})

$$\delta_{para} = \delta_{con} + \delta_{dip} \quad (2)$$

The Fermi contact shift arises from spin delocalization of the unpaired electrons to the atoms at the periphery of the molecules through chemical bonds and is directly proportional to the unpaired spin density, $\rho_{\alpha\beta}$, at each nucleus:[6]

$$\delta_{con} = \frac{\mu_0 \mu_B{}^2 g_e{}^2 (S+1)}{9kT} \rho_{\alpha\beta} \quad (3)$$

where μ_0 is the vacuum permeability, μ_B is the Bohr magneton, g_e is the free electron g-factor, S is the total spin, k is the Boltzmann constant, and T is the absolute temperature.

For the chromium compounds investigated, $S = 3/2$ so that at $T = 293$, the relationship between the Fermi contact shift expressed in ppm and the contact spin density in atomic units can be expressed as

$$\delta_{con} = 2.0051 \times 10^5 \rho_{\alpha\beta} \quad (4)$$

Estimation of Dipolar Contribution to the Chemical Shift. The Fermi contact shift term can be very large as compared to the dipolar shift (δ_{dip}), which is strongly dependent on the distance between the paramagnetic center and the nucleus and the orientation in space. For axially symmetric systems, the metal-centered pseudo-contact contribution to the chemical shift (δ^M_{dip}) can be estimated by applying the formula of Kurland and McGarvey:[17]

$$\delta^M_{dip} = \frac{S(S+1)\mu_B{}^2}{9kT} \frac{(3\cos^2\theta - 1)}{r^3} (g_{\|}{}^2 - g_{\perp}{}^2) \times \left[1 - \frac{(g_{\|}{}^2 - 0.5 g_{\perp}{}^2)}{3(g_{\|}{}^2 - g_{\perp}{}^2)} \frac{D}{kT}\right] \quad (5)$$

where $g_{\|}$ and $g_{\perp}$ are the parallel and orthogonal g-factors, D is the zero-field splitting, r is the length of the metal−nucleus vector, and θ is the angle between that vector and the magnetic (or the principal symmetry) axis. For rhombic systems, a second geometric factor also should be taken into account, but for simplicity and because this contribution is often small, axial symmetry will be assumed as a first approximation. This simplification is supported by analysis of the EPR spectra of **1**, which shows a nearly axial g-splitting.[18]

To estimate the dipolar contribution to the paramagnetic shift in the systems under study, we have calculated the maximum and minimum limit values of δ^M_{dip} for the hydrogen atoms of **1**. As a model system for the estimation of the dipolar contribution, we choose the complex biscyclopentadienyl−chromium(III) hexafluorophosphate reported by Köhler ($g_{\|} = 1.911$, $g_{\perp} = 1.785$, and $D = 1.461$ cm^{-1}).[16] In eq 5, the second term is a

(17) Kurland, R. J.; McGarvey, B. R. *J. Magn. Reson.* **1970**, *2*, 286.

(18) Fernández, P. Quinolylcyclopentadienyl Chromium Complexes as Highly Active Catalysts for Ethylene Polymerization: a Synthetic, Spectroscopic and Theoretical Approach. Ph.D. Thesis, Universidad de Oviedo, 2004.

Table 2. Calculated Maximum Ranges of Dipolar Shifts (δ_{dip}) for 1 at 373 K[a]

nucleus	r (Å)	δ_{dip} min ($\theta = 90°$)	δ_{dip} max ($\theta = 90°$)
H^2	3.07	−11.7	23.4
H^3	5.20	−2.4	4.8
H^4	5.98	−1.6	3.2
H^5	6.41	−1.3	2.6
H^6	6.44	−1.3	2.5
H^7	4.88	−2.9	5.7

[a] Reference axis of 0 and 90°, respectively, for each position. r = distance H^n−Cr (Å); for numbering of H atoms, see Figure 3.

geometrical factor, $G(r,\theta)$, which is calculated from the solid-state molecular structure data. At first sight, we cannot determine the principal magnetic axis, and therefore, the value of θ is unknown. However, we know that the maximum value of the dipolar shift is found when the reference axis is along the shortest line between the atom of interest and the paramagnetic center (at $\theta = 0°$).When the reference axis is orthogonal (at $\theta = 90°$), the minimum value is obtained. When the angle θ is 54.7 or 125.3° for a nucleus, the dipolar shift contribution is 0. The estimated upper and lower limits for dipolar shifts are summarized in Table 2. Because the dipolar shift decays with r^3,[6] the atoms close to the chromium center may have the largest shift. The atom H^2 is the closest hydrogen to the paramagnetic center, and its minimum and maximum dipolar shifts are −11.7 and +23.4 ppm, respectively.

The data in Table 2 reveal that the maximum dipolar contribution to chemical shifts for hydrogen H^2 (from −11.7 to +23.4 ppm) is considerably smaller than the Fermi contact interaction (−85 ppm). The other hydrogens show still smaller dipolar shifts, about 1 order of magnitude lower. Thus, in these Cr(III) complexes, the most important contribution to the paramagnetic shift is the Fermi contact shift (δ_{con}). Other contributions to the observed chemical shift such as ligand-centered dipolar interactions or dipolar fields originating from electron spin density on surrounding nuclei are likely to be small. As shown in eq 4, δ_{con} is proportional to the unpaired spin density $\rho_{\alpha\beta}$, which can be calculated by quantum mechanical methods. This prompted us to carry out DFT calculations to predict paramagnetic NMR chemical shifts and to provide information for in situ prepared compounds such as active chromium polymerization catalysts.

NMR Spectroscopy and DFT Calculations. For a detailed analysis of the NMR spectroscopic properties of **1**−**8**, their isotropic Fermi contact couplings were calculated by means of DFT methods.[19] All calculations were performed using the UB3LYP density functional[20] as implemented in the Gaussian 98 series of programs.[21] All geometries were optimized without any symmetry restrictions, using the experimental X-ray structures as starting points. We have tested several basis sets, selecting the all-electron 6-311g(d) basis set (see Computational Details and Supporting Information for details). In the following discussion, we will refer to the 6-311(d) basis set, if not otherwise stated.

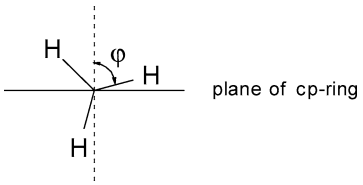

Figure 6. Side view of a CH_3 group attached to a Cp ring and dihedral angle φ.

Complex **1** was selected to check the methodology. In **1**, two fragments should be distinguished: the quinolyl moiety and the methyl groups at the Cp. While the protons at the quinoline are fixed, the CH_3 groups can rotate freely during the NMR measurement. As a result, their chemical shift values are not as indicative of the spin density distribution as are the shifts of the protons attached to the quinoline because of the unknown average rotational conformations of the methyl groups. As only one conformer structure was calculated, we chose a model[22] where the protons are considered to be in fixed orientations and the observed contact spin density is obtained by introduction of a correction factor called angular dependence, $R(\varphi) = A + B\cos^2(\varphi)$, where A and B are empirical parameters and φ is the angle between the methyl C−H bond vector and the orthogonal of the Cp ligand plane (Figure 6).

As A is negligible in comparison to $B\cos^2(\varphi)$, the effective contact spin density at each methyl group arises from the average of the corrected contact spin density from the hydrogens

$$\rho_{\alpha\beta} = 1/3\Sigma(B\cos^2(\varphi)\rho_{\alpha\beta(\mathrm{calc})}) \qquad (6)$$

For the 6-31g basis set, the experimental paramagnetic shift was plotted against the computed spin density, obtaining a linear correlation ($r^2 = 0.9935$) for the quinolyl hydrogens. On the other hand, the calculated contact spin densities at the methyl groups are in both cases negative, whereas the experiment shows positive and negative signs. Only when polarization *d*-functions at the heavy atoms were added, we observed satisfactory values for the sign of the spin density at the CH_3 groups. In the case of the 6-311G(d) basis set, a good linear correlation results, including the methyl hydrogens ($r^2 = 0.9747$). The B value was set to 1.0. The slope is 1.8862×10^5, and the intercept is 6.0 ppm. Thus, to qualitatively reproduce the experimental trends for the H atoms of the methyl substituents, the inclusion of polarization functions at heavy elements was required. On the other hand, adding polarization functions at the hydrogen atoms or diffuse functions at heavy atoms did not lead to better results.

Table 3 summarizes the correlation between calculated contact spin densities at the UB3LYP/6-311g(d) level with the observed paramagnetic shifts. When the observed paramagnetic shift values of all these molecules are plotted against the computed contact spin density (Figure 7), a good linear regression is obtained ($r^2 = 0.9724$). The slope is 1.8480×10^5, and the

(19) For more comprehensive calculations of chemical shifts of paramagnetic molecules, see: (a) Moon, S.; Patchkovskii, S. In *Calculation of NMR and EPR Parameters: Theory and Applications*; Kaupp, M., Bühl, M., Malkin, V. G., Eds.; Wiley-VCH: Weinheim, Germany, 2004. (b) Telyatnyk, L.; Vaara, J.; Rinkevicius, Z.; Vahtras, O. *J. Phys. Chem. B* **2004**, *108*, 1197 and references cited therein.

(20) (a) Becke, A. D. *J. Chem. Phys.* **1993**, *98*, 5648. (b) Lee, C.; Yang, W.; Parr, R. G. *Phys. Rev. B* **1998**, *37*, 785.

(21) Frisch, M. J.; Trucks, G. W.; Schlegel, H. B.; Scuseria, G. E.; Robb, M. A.; Cheeseman, J. R.; Zakrzewski, V. G.; Montgomery, J. A., Jr.; Stratmann, R. E.; Burant, J. C.; Dapprich, S.; Millam, J. M.; Daniels, A. D.; Kudin, K. N.; Strain, M. C.; Farkas, O.; Tomasi, J.; Barone, V.; Cossi, M.; Cammi, R.; Mennucci, B.; Pomelli, C.; Adamo, C.; Clifford, S.; Ochterski, J.; Petersson, G. A.; Ayala, P. Y.; Cui, Q.; Morokuma, K.; Malick, D. K.; Rabuck, A. D.; Raghavachari, K.; Foresman, J. B.; Cioslowski, J.; Ortiz, J. V.; Baboul, A. G.; Stefanov, B. B.; Liu, G.; Liashenko, A.; Piskorz, P.; Komaromi, I.; Gomperts, R.; Martin, R. L.; Fox, D. J.; Keith, T.; Al-Laham, M. A.; Peng, C. Y.; Nanayakkara, A.; Challacombe, M.; Gill, P. M. W.; Johnson, B.; Chen, W.; Wong, M. W.; Andres, J. L.; Gonzalez, C.; Head-Gordon, M.; Replogle, E. S.; Pople, J. A. *GAUSSIAN 98*, revision A.9; Gaussian, Inc.: Pittsburgh, PA, 1998.

(22) (a) Heller, C.; McConnell, H. M. *J. Chem. Phys.* **1960**, *32*, 1535. (b) Stone, E. W.; Maki, A. H. *J. Chem. Phys.* **1962**, *37*, 1326. (c) La Mar, G. N.; Van Hecke, G. R. *J. Chem. Phys.* **1970**, *52*, 5676. (d) Zakharieva, O.; Schünemann, V.; Gerdan, M.; Licoccia, S.; Cai, S.; Walker, F. A.; Trautwein, A. X. *J. Am. Chem. Soc.* **2002**, *124*, 6636.

Table 3. Obtained Correlation between Calculated Contact Spin Densities at UB3LYP/6-311g(d) and Observed Paramagnetic Shifts in Quinolyl−Cp−Chromium(III) Complexes 1−8

		quinoline		total	
complex	no. of basis functions	correlation (r^2)	slope ($\times 10^5$)	correlation (r^2)	slope ($\times 10^5$)
$Cp^{*Q}CrCl_2$ (**1**)	494	0.9982	1.8021	0.9762	1.8717
$Cp^{*Qd}CrCl_2$ (**2**)	518	0.9938	2.2116	0.9871	2.1711
$Cp^{Q}CrCl_2$ (**3**)	398	0.9975	1.7828	*a*	
$Cp^{*Q}CrBr_2$ (**4**)	530	0.9931	1.6805	0.9772	1.8234
$Cp^{IIIQ}CrCl_2$ (**5**)	470	0.9986	1.7927	0.9778	1.8547
$Cp^{*SiQ}CrCl_2$ (**6**)	574	0.9944	1.8007	0.9830	1.7379
$Cp^{*SiQ}Cr(OTf)_2$ (**7**)	826	0.9956	1.6792	0.9919	1.6935
$Cp^{*Q}Cr(CH_3)Cl$ (**8**)	495	0.9978	1.6862	0.9626	2.0465

[a] No satisfactory results were obtained for the Cp−H atoms.

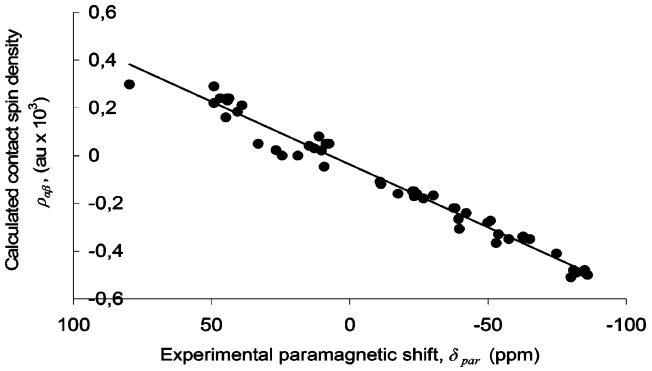

Figure 7. Paramagnetic shift vs contact spin density at hydrogen atoms in complexes **1**−**8** calculated with UB3LYP/6-311g(d).

intercept is only 6.4 ppm. This is in fairly good agreement with the theoretical value of 2.0051×10^5 (see eq 5). The stronger deviations arise from the signals of the methyl groups, especially from those adjacent to the quinoline ring. This can be due to a possible minor dipolar shift contribution. These results indicate that the Fermi contact shift dominates the paramagnetic shifts and that the theoretical predictions reproduce the experimental results.

The results of the calculation show that the chlorine atoms bear a positive spin density. This pattern has been previously reported for other chromium compounds.[7] The accumulation of positive spin density at the chlorine ligands stems from interaction of the chlorine lone pairs with d orbitals of the chromium atom, which leads to a delocalization of the positive spin (i.e., the unpaired electron in the SOMO) to the chlorine atoms. This is easily visible from an analysis of the SOMOs in **1**. All three singly occupied orbitals have large coefficients at the chlorine atoms. The nitrogen atom carries a negative spin density due to the typical polarization of the Fermi contact interaction. The carbon atoms of the quinoline have either a positive or a negative spin density, with the signs alternating on most adjacent atoms, as expected for paramagnetic molecules.

As described previously, the methyl−chloro complex **8** was characterized by ^{1}H NMR and compared with the dichloro derivative **1**. The resonances are further apart from the diamagnetic region than those of **1**. This fact is reproduced by the calculated contact spin densities of the geometry-optimized molecule (Table 4). For all hydrogen atoms, the absolute value of the contact spin density at the nuclei is higher than in **1**. The values are particularly different at the methyl groups. The unpaired electron spin densities at the hydrogens of the $CpCH_3$ groups located at a trans position relative to the $Cr-CH_3$ group is very high so that a strongly shifted NMR resonance should

Table 4. Paramagnetic Shifts and Contact Spin Densities at Hydrogen Atoms in 8 Calculated with UB3LYP/6-311g(d)[a]

nucleus	exptl[b] paramagnetic shift (ppm)	calcd contact spin density, $\rho_\alpha\beta$, (au $\times 10^3$)
H^2	*c*	−0.580
H^3	48.0	0.290
H^4	−87.0	−0.500
H^5	−27.7	−0.180
H^6	10.1	0.080
H^7	−12.0	−0.110
H^8	167.0	0.655
H^9	−54.0	−0.367
H^{10}	39.5	0.183
H^{11}	36.0	0.049
Me	*c*	6.580[d]

[a] For numbering in **8**, see Figure 5. [b] Values are corrected by subtraction of the diamagnetic shift: +8 ppm for $H^2 - H^7$ and +2 ppm for CH_3 groups. [c] Not observed. [d] Average value.

result. Indeed, this is the case for one CH_3 group in the ^{1}H NMR of **8** (observed 168 ppm and predicted 146 ppm, see Figure 5 and Table 4). Figure 8 depicts the calculated spin density distribution for **1** and **8**.

The results of the DFT calculations allow for the spectral assignment, which was not easily achieved from the experimental NMR spectroscopic data. For example, in **1**, it is possible to assign the signal at −15.8 ppm (which means $\delta_{para} = -23.8$ ppm) to H^5 and not to H^7. The calculated contact spin densities of the H^5 and H^7 atoms can be converted into chemical shifts using the slope and intercept values of the overall linear correlation. The obtained values are −14.6 and 0.2 ppm for H^5 and H^7, respectively. Clearly, the theoretical value of H^5 fits qualitatively, if not quantitatively, to the experimental chemical shift, whereas H^7 does not. Likewise, for the other complexes **2**−**8**, the signals appearing in the range between −15 and −20 ppm can be assigned to the H^5 atom. H^7 is not detected for **1**−**7**, for which the theoretical shifts are between 5.7 and −1.7 ppm, respectively. If we consider an additional small dipolar contribution to the overall shift, the signal may be shifted further into the diamagnetic region. The possible dipolar contributions to the shifts will be discussed in more detail next.

The difficult assignment of the protons of methyl substituents on **8** was also achieved with the help of DFT calculations. As can be seen in Table 5, there is generally good agreement with the assignments proposed: CH_3^8 has the largest downfield shift, 168 ppm from experiment, in good accord with the 146 ppm computed Fermi shift. The peaks at −52, 41, and 38 ppm are attributed to CH_3^9, CH_3^{10}, and CH_3^{11}, respectively, on the basis of their calculated Fermi shifts of −62, 41, and 16 ppm, respectively.

No significant differences between calculated distances and angles and those from the experimental solid-state geometry were observed except in the trimethylsilyl derivate **6**. In this case, optimization leads to a molecular geometry where the angle between the quinoline and the Cp ring is nearly 90°, whereas in the solid state, an angle of 68.9° was determined.

Despite the significant differences of the methyl environment in the calculated as compared to crystallographic geometries, a good correlation between experimental paramagnetic shift and calculated contact spin densities in **6** ($r^2 = 0.9830$) is found. Barone reported that small geometry changes can strongly affect the spin density.[23] To determine whether the almost 90° angle between the quinoline and the Cp ring or a geometry closer to the experimental solid-state molecular structure is present in solution, a new geometry optimization of **6** was performed with

(23) Improta, R.; Barone, V. *Chem. Rev.* **2004**, *104*, 1231.

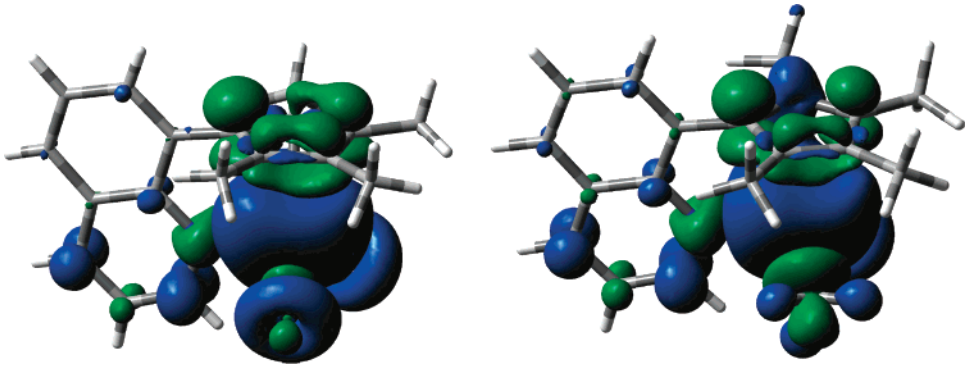

Figure 8. Plot of the calculated unpaired spin density in complexes **1** (left) and **8** (right). Blue is positive and green is negative unpaired spin density.

Table 5. Comparison of Experimental Paramagnetic Chemical Shifts of 1−8 with Calculated Shifts (in Brackets) Using Eq 1 and $\delta_{con} = 1.8484 \times 10^5 \rho_{\alpha\beta} + 6.1$ ppm

	δ_{para} (exptl) (ppm)[a] [δ_{para} (calcd)]						
complex	$Me^{8/11}$[b]	$Me^{9/10}$[b]	H^2	H^3	H^4	H^5	H^6
$Cp^{*Q}CrCl_2$ (**1**)	25.6	−43.1	−86	43.8	−64.0	−23.8	7.3
	[10.4]	[−38.4]	[−84.5]	[50.5]	[−58.6]	[−21.6]	[15.3]
$Cp^{*Q}dCrCl_2$ (**2**)	23.4	−75.8	78.7[c]	43.7	−39.1	−12.3	11.7
	[6.0]	[−69.8]	[61.2][c]	[35.7]	[−34.6]	[−16.1]	[11.6]
$Cp^{Q}CrCl_2$ (**3**)	248[d]	208[d]	−81	48.0	−54.8	−18.5	15.6
	[152]	[150]	[−88]	[47]	[−54.9]	[−23.5]	[13.5]
$Cp^{*Q}CrBr_2$ (**4**)[e]	8.2	−51.9	−82	43.3	−66.1	−25.2	7.5
	[−2.5]	[−44.3]	[−83]	[50.5]	[−58.6]	[−23.5]	[15.3]
$Cp^{IIIQ}CrCl_2$ (**5**)	17.7	−38.7	−86	42.6	−63.6	−24.4	7.2
	[6.0]	[−34.4]	[−83]	[50.5]	[−56.7]	[−21.6]	[15.3]
$Cp^{*SiQ}CrCl_2$ (**6**)	9.2	−31.3, −40.7	−83	43.1	−63.9	−24.7	7.6
	[10.0]	[−24.8, −50.8]	[−84]	[48.6]	[−56.7]	[−23.3]	[15.3]
$Cp^{*SiQ}Cr(OTf)_2$ (**7**)	*f*	−40.9, −50.9	*f*	37.9	−58.6	−24.3	6.4
	[−0.3]	[−43.0, −45.8]	[−75]	[44.9]	[−58.6]	[−25.3]	[15.3]
$Cp^{*Q}Cr(CH_3)Cl$ (**8**)	167, 36	−54, 39.5	*f*	48.0	−87.0	−27.7	10.1
	[127, 15.2]	[−61.7, 39.2]	[−101]	[59.7]	[−86.3]	[−27.2]	[20.9]

[a] $CDCl_3$, 200 MHz, d1 = 0.3 ms, lb = 10 Hz, SW = 375 ppm, and NS = 1000−3000. The diamagnetic shift was substracted from the experimental value (+8 ppm for aromatic H and +2 ppm for CH_3). [b] Average value using eq 6 with $B = 1.0$. [c] Methyl group of the quinoline. [d] Hydrogen atoms of C_5H_4R. [e] Measured in CD_2Cl_2. [f] Not observed.

the C2−C1−C10−C11 dihedral angle frozen to the experimentally determined value of −68.9° (see Supporting Information). Now, the calculated structure differs less from the experiment. However, this new optimized geometry gives a spin density distribution that does not correlate well with the ^{1}H NMR shifts. (A worse linear correlation with $r^2 = 0.8458$ is obtained.) This leads to the conclusion that the geometry of **6** in solution is closer to the calculated (i.e., angle of quinoline−Cp = 90°) than to the structure in the solid state, in which packing effects could play a significant role.

In general, the trends of the experimental NMR shifts are well-reproduced by the calculations of the contact spin densities. However, some quantitative values represent non-negligible deviations from the experimental data. In particular, this applies to H^7 of the quinolyl moiety and the methyl groups adjacent to the quinoline substituent. These discrepancies are due to non-negligible contributions of the dipolar shift. As outlined previously for a simplified axial system (see Table 2), the dipolar contribution to ^{1}H NMR shifts depends on the orientation and length of the metal-to-hydrogen vector. Therefore, only the atoms H^2, H^3, and H^7 may have considerable dipolar shifts. As the atom H^2 has the smallest distance from the chromium center, the difference between calculated and experimental NMR shift can be used for measuring the dipolar contribution to the NMR shift of that H atom, and hence, the orientation metal-centered magnetic axis can be estimated. This leads to an orientation as drafted in Figure 9. In this figure, the area of the minimum dipolar shift is represented by the surface of a double cone.

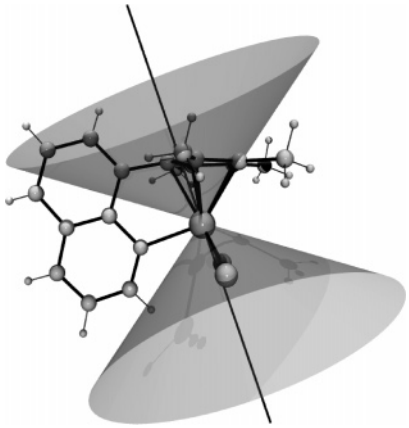

Figure 9. Magnetic axis and double cones with a simplified model for **1**. Cone surfaces represent the area where dipolar interactions are zero (54.7° angle).

The H atoms that lie close to the surface should experience a minimum dipolar shift. Therefore, the experimental paramagnetic NMR shift for the signal H^2 is well in accordance with the calculated contact spin density on that position. However, H atoms that are close to the Cr atom and lie along or orthogonal to the magnetic axis should experience a greater dipolar shift. The atom H^7 lies in the double cone and has therefore a positive dipolar shift. The calculated Fermi contact contribution for H^7 is −7 ppm. If we add the diamagnetic contribution (+8 ppm) and a small positive dipolar contribution (2−4 ppm), the signal

for that atom should resonate in the 0−10 ppm region and is difficult to identify due to residual solvent signals and diamagnetic impurities. Therefore, we were not able to assign experimental NMR signals to H^7. As explained previously, the dipolar contribution is not significant at other quinolyl protons because they are too far apart. We predict small contributions (0.8 to −1.6 ppm), positive for H^5 and negative for H^3, H^4, and H^6.

Conclusion

DFT calculations on paramagnetic quinolyl-functionalized Cp−chromium(III) complexes yield information on spin densities at hydrogen atoms and hence the Fermi contact shifts. The good correlation between calculated and experimental values indicates that the NMR hyperfine shifts are dominated by the Fermi contact shift. The results give detailed information about the spin density distribution in the metal complexes. The theoretical methodology has also led to a complete spectral assignment. The difficult assignment of methyl substituents in **8** has been completed with the support of the calculations. Deviations between the calculated NMR shifts, based on the calculated contact spin densities and the experimental NMR data, could result from dipolar shift contributions. These differences can be used to gauge the contribution of the dipolar shift to the overall shift, as well as to determine the orientation of the magnetic axis in a simplified axial model.

The calculated hyperfine shifts give remarkably good agreement with the NMR experiment. Therefore, it is now possible to investigate new paramagnetic reaction products by NMR and to determine the structure in solution by calculation of the spin delocalization and comparison with the experimental NMR values. Consequently, this technique will lead to a better understanding of paramagnetic catalysts in general and on single-site chromium-based olefin polymerization catalysts in particular.

Experimental Procedures

All manipulations were carried out under a nitrogen atmosphere with anhydrous solvents saturated with nitrogen. Glassware was heated under vacuum prior to use. The compounds **1**, **3**, **9H**,[11a] **2**,[4b] 8-bromoquinoline,[24] 2,3,4-trimethylcyclopent-2-enone,[25] [$CrBr_3$-$(THF)_3$],[26] [$CrCl_3(THF)_3$],[27] and [$CrCl_2CH_3(THF)_3$][14] were prepared according to procedures described previously. All other reagents were used as purchased.

2,3,4-Trimethyl-1-(8-quinolyl)cyclopentadiene (12H). A solution of 8-bromoquinoline (8.3 g, 40.0 mmol) in 100 mL of THF was cooled to −80 °C, and 16 mL of a 2.5 M solution of *n*-butyllithium in hexane (40.0 mmol) was added with stirring within 20 min. After stirring for another 15 min at −80 °C, 2,3,4-trimethylcyclopent-2-enone (4.96 g, 40.0 mmol) was added dropwise. The mixture was allowed to warm to room temperature and was then heated to reflux for 30 min. After cooling down, 20 g of ice and 10 mL of concentrated hydrochloric acid were added, and the mixture was stirred for 30 min. Aqueous ammonia was added until a pH of 9 was reached. The phases were separated, and the aqueous phase was subsequently extracted with diethylether (2 × 150 mL). From the combined organic layers, the solvents were evaporated in a vacuum. The crude product was purified by distillation at 117−132 °C/10^{-2} mbar to give **12H** (yellow oil): yield 4.02 g (17.1 mmol, 43%). ^{1}H NMR ($CDCl_3$, 200.13 MHz): δ 1.81 (s, 3H, CH_3), 1.82 (s, 3H, CH_3), 1.94 (s, 3H, CH_3), 3.48 (s, 2H, CH_2), 7.26 (dd, $^3J(H^3, H^4) = 8.3$ Hz, $^3J(H^3, H^2) = 4.2$ Hz, 1H, H^3), 7.43 (m, 2H, H^5/H^7), 7.61 (dd, $^3J(H, H) = 6.2$ Hz, $^3J(H, H) = 3.3$ Hz, 1H, H^6), 8.05 (dd, $^3J(H^4, H^3) = 8.3$ Hz, $^4J(H^4, H^2) = 1.9$ Hz, 1H, H^4), 8.82 (dd, $^3J(H^2, H^3) = 4.2$ Hz, $^4J(H^2, H^4) = 1.9$ Hz, 1H, H^2). ^{13}C NMR ($CDCl_3$, 50.1 MHz): δ 11.6, 13.3, 13.9 (CH_3), 49.2 (CH_2), 121.0, 126.3, 126.4, 130.2, 136.4, 149.8 (CH_{Ar+Cp}), 129.0, 135.3, 136.8, 136.9, 138.3, 141.3, 147.4 (quat. C_{Ar+Cp}). EI-MS: (*m*/*z*) 234 (100%, $M^+ - H$), 220 (59%, $M^+ - CH_3$), 204 (27%, $M^+ - CH_3 - CH_4$).

3,4,5-Trimethyl-1-(8-quinolyl)-2-trimethylsilylcyclopentadiene (13H). A solution of 2,3,4-trimethyl-1-(8-quinolyl)cyclopentadiene (**12H**) (0.87 g, 3.7 mmol) in 20 mL of THF was added to a suspension of KH (0.15 g, 3.7 mmol) in 30 mL of THF and was stirred at room temperature for 6 h. The reaction mixture turned violet, and a red precipitate was formed. Trimethylsilylchloride (0.40 g, 3.7 mmol) was added dropwise, and the mixture was stirred for 30 min. The volatile components were removed in a vacuum, and the crude product was purified by distillation at 126−136 °C/10^{-2} mbar to give **13H** (yellow oil): yield 0.46 g (1.5 mmol, 40%). ^{1}H NMR ($CDCl_3$, 200.13 MHz): δ −0.51 (s, 9H, $Si(CH_3)_3$), 1.89 (s, 3H, CH_3), 1.97 (s, 3H, CH_3), 2.04 (s, 3H, CH_3), 4.47 (s, 1H, Cp*H*), 7.25 (dd, $^3J(H^3, H^4) = 8.3$ Hz, $^3J(H^3, H^2) = 4.2$ Hz, 1H, H^3), 7.42−7.46 (m, 2H, H^5/H^7), 7.60 (m, 1H, H^6), 8.03 (dd, $^3J(H^4, H^3) = 8.3$ Hz, $^4J(H^4, H^2) = 1.9$ Hz, 1H, H^4), 8.83 (dd, $^3J(H^2, H^3) = 4.2$ Hz, $^4J(H^2, H^4) = 1.9$ Hz, 1H, H^2). ^{13}C NMR ($CDCl_3$, 50.1 MHz): δ −2.1 ($Si(CH_3)_3$), 11.7, 13.2, 15.3 (CH_3), 55.9 (CH_{Cp}), 120.8, 126.2, 126.4, 130.7, 136.3, 149.7 (CH_{Ar}), 129.0, 135.9, 136.4, 138.3, 138.6, 139.2, 148.4 (quat. C_{Ar+Cp}). EI-MS: (*m*/*z*) 307 (26%, M^+), 292 (70%, $M^+ - CH_3$), 234 (100%, $M^+ - Si(CH_3)_3 - CH_3$).

Dibromo-η^5-[2,3,4,5-tetramethyl-1-(8-quinolyl)cyclopentadienyl]chromium (III) (4). A solution of 2,3,4,5-tetramethyl-1-(8-quinolyl)cyclopentadiene (**9H**) (0.27 g, 1.1 mmol) in 20 mL of THF was added to a suspension of KH (0.05 g, 1.1 mmol) in 10 mL of THF. The mixture turned violet. After 12 h at room temperature, the reaction mixture was slowly added to a solution of [$CrBr_3$-$(THF)_3$] (0.56 g, 1.1 mmol) in 20 mL of THF. After stirring for 6 h, the solvent was evaporated in vacuum, and the residue was washed twice with 30 mL of hexane and extracted with hot toluene (3 × 50 mL). After evaporation of the toluene, **4** was obtained as a green powder: yield 0.36 g (0.8 mmol, 72%). ^{1}H NMR (CD_2Cl_2, 200.13 MHz): δ −74 (1H, H^2), −58.1 (1H, H^4), −48.9 (6H, $CH_3^{9/10}$), −17.2 (1H, H^5), 11.2 (6H, $CH_3^{8/11}$), 15.5 (1H, H^6), 51.3 (1H, H^3). EI-MS: (*m*/*z*) 460 (35%, M^+), 381 (100%, $M^+ - Br$), 297 (23%, $M^+ - 2HBr$), 246 (20%, $M^+ - 2HBr - Cr$). UV/vis (THF): $\lambda_{max}(\epsilon)$ 470 (231), 649 (305) nm. Anal. calcd for $C_{18}H_{18}NCrBr_2$: C, 46.98 (47.52); H, 3.94 (4.16); N, 3.04 (2.98).

Dichloro-η^5-[2,3,4-trimethyl-1-(8-quinolyl)cyclopentadienyl]chromium(III) (5). The synthesis is analogous to the preparation of **4**, from 0.14 g (0.6 mmol) of **12H**, 0.03 g (0.6 mmol) of KH, and 0.23 g (0.6 mmol) of [$CrCl_3(THF)_3$]. The product is less soluble than **4**, so that it was extracted 5 times with 50 mL of toluene. After evaporation of the toluene, **5** was obtained as a green powder: yield 0.07 g (0.2 mmol, 30%). ^{1}H NMR ($CDCl_3$, 200.13 MHz): δ −78 (1H, H^2), −55.6 (1H, H^4), −34.7 (6H, $CH_3^{9/10}$), −16.4 (1H, H^5), 15.3 (1H, H^6), 20.7 (3H, CH_3^8), 50.6 (1H, H^3). EI-MS: (*m*/*z*) 356 (72%, M^+), 320 (100%, $M^+ - HCl$), 284 (24%, $M^+ - 2HCl$), 232 (26%, $M^+ - 2HCl - Cr$). UV/vis (THF): $\lambda_{max}(\epsilon)$ 469 (359), 700 (447) nm. Anal. calcd for $C_{17}H_{16}NCrCl_2$: C, 57.16 (57.04); H, 4.51 (4.56); N, 3.92 (3.89).

Dichloro-η^5-[3,4,5-trimethyl-1-(8-quinolyl)-2-trimethylsilylcyclopentadienyl]chromium(III) (6). The synthesis is analogous to the preparation of **4**, from 0.12 g (0.4 mmol) of **13H**, 0.02 g (0.4 mmol) of KH, and 0.15 g (0.4 mmol) of [$CrCl_3(THF)_3$]. After evaporation of the toluene, **6** was obtained as a green powder: yield 0.11 g (0.3 mmol, 65%). ^{1}H NMR ($CDCl_3$, 200.13 MHz): δ −75

(24) Mirek, J. *Roczniki Chem.* **1960**, *34*, 1599.
(25) Broussier, R.; Ninoreille, S.; Legrand, C.; Gautheron, B. *J. Organomet. Chem.* **1997**, *532*, 55.
(26) Jones, P. J.; Hale, A. L.; Levason, W.; McCullough, F. P., Jr. *Inorg. Chem.* **1983**, *22*, 2642.
(27) Heyn, B.; Hipler, B.; Kreisel, G.; Schreer, H.; Walther, D. *Anorganische Synthesechemie*; Springer-Verlag: Berlin, 1990; p 23.

Table 6. Crystal Data and Structure Refinement Details for 4−8

	4	5	6	7	1 + 8
empirical formula	$C_{18}H_{18}Br_2CrN$	$C_{17}H_{16}Cl_2CrN$	$C_{20}H_{24}Cl_2CrNSi$	$C_{22}H_{24}CrF_6NO_6S_2Si$	$C_{18.4}H_{19.1}Cl_{1.6}CrN$
fw	460.15	357.21	429.39	656.63	363.57
cryst syst	monoclinic	monoclinic	triclinic	monoclinic	orthorhombic
space group	$P2_1/n$	$P2_1/c$	$P\bar{1}$	$P2_1/c$	Pbca
a (Å)	13.5735(9)	11.8000(5)	8.6425(5)	13.859(3)	14.014(2)
b (Å)	17.4864(11)	8.9527(4)	10.0291(6)	11.248(2)	13.807(2)
c (Å)	15.5798(10)	14.6019(6)	13.5776(9)	18.424(4)	17.520(2)
α (deg)	90	90	97.051(1)	90	90
β (deg)	111.054(1)	93.790(1)	100.808(1)	105.970(4)	90
γ (deg)	90	90	114.190(1)	90	90
V (Å^3)	3451.0(4)	1539.20(11)	1027.98(11)	2761.1(9)	3389.8(5)
Z	8	4	2	4	8
calcd density (g/cm^3)	1.771	1.541	1.387	1.580	1.425
abs coeff (mm^{-1})	5.290	1.081	0.878	0.687	0.926
F(000)	1816	732	446	1340	1496
cryst size (mm)	0.36 × 0.14 × 0.12	0.36 × 0.30 × 0.22	0.28 × 0.11 × 0.02	0.35 × 0.28 × 0.27	0.60 × 0.35 × 0.02
θ range for data collection (deg)	1.71−27.48	1.73−32.03	1.57−28.36	2.14−32.01	2.37−25.01
no. of rflns collected	37847	16673	15075	29129	16201
no. of independent rflns (R(int))	7850(0.053)	5161(0.0295)	5133(0.0544)	9092(0.0315)	2939(0.0404)
params	541	254	322	448	274
GOF (F^2)	1.023	1.066	1.047	1.038	1.098
R1	0.0340	0.0317	0.0423	0.0315	0.0494
wR2	0.0883	0.0899	0.1167	0.0854	0.1233
largest diff peak and hole (e Å^{-3})	1.224 and −0.435	0.710 and −0.493	0.484 and −0.541	0.511 and −0.439	0.537 and −0.573

(1H, H^2), −56.9 (1H, H^4), −36.7, −27.3 (6H, $CH_3^{9/10}$), −16.7 (1H, H^5), 12.2 (3H, CH_3^8), 15.7 (1H, H^6), 51.1 (1H, H^3). EI-MS: (*m*/*z*) 428 (84%, M$^+$), 392 (100%, M$^+$ − HCl), 356 (9%, M$^+$ − 2HCl). UV/vis (THF): $\lambda_{max}(\epsilon)$ 475 (493), 695 (747) nm. Anal. calcd for $C_{20}H_{24}NCrCl_2Si$: C, 55.94 (56.48); H, 5.63 (5.80); N, 3.26 (3.41).

Bistrifluoromethanesulfonato-η^5-[3,4,5-trimethyl-1-(8-quinolyl)-2-trimethylsilyl-cyclopentadienyl]chromium(III) (7). Silver trifluoromethylsulfonate (0.63 g, 2.5 mmol) was added to a solution of dichloro-η^5-[3,4,5-trimethyl-1-(8-quinolyl)-2-trimethylsilyl-cyclopentadienyl]chromium(III) (**6**) (0.53 g, 1.2 mmol) in 30 mL of CH_2Cl_2.The mixture was stirred at room temperature for 30 min. The solvent was evaporated in a vacuum, and the residue was washed with hexane (3 × 30 mL) and extracted with toluene (2 × 20 mL). After evaporation of the toluene, **7** was obtained as a blue−green powder: yield 0.62 g (1.0 mmol, 72%). ^{1}H NMR ($CDCl_3$, 200.13 MHz): δ −50.6 (1H, H^4), −42.9, −32.4 (6H, $CH_3^{9/10}$), −16.3 (1H, H^5), 15.7 (1H, H^6), 51.1 (1H, H^3). EI-MS: (*m*/*z*) 656 (82%, M$^+$), 641 (90%, M$^+$ − CH_3), 506 (100%, M$^+$ − SO_2CF_3 − 2H). UV/vis (THF): $\lambda_{max}(\epsilon)$ 451 (184), 626 (459) nm.

Chloromethyl-η^5-[2,3,4,5-tetramethyl-1-(8-quinolyl)cyclopentadienyl]chromium(III) (8). A solution of 2,3,4,5-tetramethyl-1-(8-quinolyl)cyclopentadiene (**9H**) (0.37 g, 1.5 mmol) in 5 mL of THF was added to a suspension of KH (0.06 g, 1.5 mmol) in 10 mL of THF. The mixture turned violet. After 6 h at room temperature, the reaction mixture was slowly added to a solution of [$CrCl_2CH_3(THF)_3$] (0.53 g, 1.5 mmol) in 20 mL of THF. After stirring for 12 h, the solvent was evaporated in a vacuum, and the residue was extracted with hot toluene (6 × 20 mL). After evaporation of the toluene, purple crystals of **8** together with **1** were obtained. ^{1}H NMR ($CDCl_3$, 200.13 MHz): δ −79.0 (1H, H^4), −52 (3H, CH_3^9), −19.7 (1H, H^5), −4.0 (1H, H^7), 18.1 (1H, H^6), 34.0 (3H, CH_3^{11}), 41.5 (3H, CH_3^{10}), 56.0 (1H, H^3), 169 (3H, CH_3^8).

NMR Studies. The NMR spectra were recorded with a Bruker DRX 200 (200.1 MHz for ^{1}H NMR) spectrometer by using solutions in chloroform-d_1 or dichloromethane-d_2. All signals were calibrated relative to residual solvent peaks. If not otherwise stated, the temperature was 295 K. The following parameters were used: sweep width: 300 ppm; 90° ^{1}H-pulse (12.6 μs) relaxation delay: 0.3 ms; data points in time domain: 32 768; acquisition time: 0.27 s; 1024 repetitions; and exponential window function with 10 Hz line broadening.

Computational Details. All calculations were performed using the spin unrestricted hybrid B3LYP density functional[20] as implemented in the Gaussian 98 series of programs.[21] Because of the size of the system, several basis sets were tested to obtain a good combination of accuracy and computational efficiency. The checking included the LanL2DZ,[28,29] 6-31g,[29] 6-31g(d),[29] 6-31g(d,p),[29] 6-311g(d),[29] and 6-311+g(d) basis sets. In addition, the locally dense scheme[10b] consisting of a Watchers' basis set for chromium,[30] 6-311g(d) for the other heavy atoms, and 6-31g(d) for the hydrogen atoms was tested. Such a scheme was proposed to reproduce spin populations on metalloporphyrin systems.[10b]

The calculation of the Fermi contact coupling constants on **1** was used to back up our methodology. The overall linear regression between experimental hyperfine shifts and Fermi contact spin densities for the LANL2DZ and 6-31g basis set showed low slopes (1.31×10^5 and 1.21×10^5, respectively, vs the theoretical 2.00×10^5) and R^2 values lower than 0.9. The use of the all-electron basis set 6-311g(d) including polarization functions at the heavy atoms significantly improved the results leading to a better linear correlation ($R^2 = 0.9747$) and to a slope value of 1.8862×10^5 closer to the theoretical value. These results indicate that all-electron basis sets, as well as polarization functions, are required to obtain satisfactory results. Additionally, we considered the effect of adding polarization functions at hydrogen atoms (6-31g(d,p)), diffuse functions at heavy elements 6-311+g(d), and using the locally dense scheme. None of these basis sets caused dramatic changes either in the slope (1.6898×10^5, 1.9022×10^5, and 1.7926×10^5, respectively) or in the R^2 values (0.9696, 0.9644, and 0.9725). Finally, the 6-311g(d) basis set was selected as a compromise between accuracy and computational efficiency. Geometry optimizations were carried out without any symmetry restrictions, and all stationary points were optimized with analytical first derivatives. The convergence in these open shell systems showed some difficulties, and therefore, special measures were required. To avoid the oscillatory behavior of the SCF procedure, we used a virtual orbital shift of 300 mHartrees. To overcome the poor initial semiempirical guess, we performed the calculation at lower levels of theory, and then we used the final wave function as a starting point for UB3LYP/6-311g(d) calculations. During all the calculations, the spin contamination was carefully controlled. The values

(28) Hay, P. J.; Wadt, W. R. *J. Chem. Phys.* **1985**, *82*, 299.
(29) (a) Francl, M. M.; Pietro, W. J.; Hehre, W. J.; Binkley, J. S.; Gordon, M. S.; Defrees, D. J.; Pople, J. A. *J. Chem. Phys.* **1982**, *77*, 3654. (b) Hehre, W. J.; Ditchfield, R.; Pople, J. A. *J. Chem. Phys.* **1972**, *56*, 2257. (c) Hariharan, P. C.; Pople, J. A. *Theor. Chim. Acta* **1973**, *28*, 213.
(30) (a) Wachters, A. J. H. *J. Chem. Phys.* **1970**, *52*, 1033. (b) Wachters, A. J. H. *IBM Technology Report RJ584*; 1969.

of $\langle S^2 \rangle$ only slightly deviated from the expected value of 3.75. Additionally, the atomic spin populations were obtained following the Mulliken population scheme.

X-ray Crystal Structure Determinations of 4−8. Crystal data for **4**−**8** were collected on a Bruker AXS SMART 1000 diffractometer with a CCD area detector (Mo Kα radiation graphite monochromator, $\lambda = 0.71073$ Å) at −83 °C (**4**−**6**), −167 °C (**7**), and −100 °C (**8**). An absorption correction (semiempirical from equivalents) was applied.[31] The structures were solved by direct methods and refined by full-matrix least-squares against F^2 with all reflections using the SHELXTL programs.[32] All hydrogen atoms (except those for **8**) were located in difference Fourier maps and refined isotropically. Crystal data and experimental details are listed in Table 6.

(31) Sheldrick, G. M. *SADABS*, version 2.01; University of Göttingen: Göttingen, Germany, 2000.

(32) Sheldrick, G. M. *SHELXTL NT*, version 5.1; Bruker AXS: Madison, WI, 1999.

Acknowledgment. We thank the Deutsche Forschungsgemeinschaft (Sonderforschungsbereich 623) for financial support and the Graduate College 850 for the availability of computer resources.

Supporting Information Available: Complete crystal data and tables for the structures of **4**−**8** and for $CrCl_2(CH_3)(thf)_3$ and paramagnetic ^1H NMR spectra of **2**, **3**, and **5**. This material is available free of charge via the Internet at http://pubs.acs.org.

OM070173Y